Regulation of Te oxide layer on a CdZnTe film for adjusting surface contact of a CdZnTe-based device

Zilong Zhang[1, 2, *], Keyun Gu[1], Tianyu Zou[1], Jian Huang[1, 3 *], Ke Tang[1], Yue Shen[1], Haitao Ye[4], Meiyong Liao[2], and Linjun Wang[1, 3]

[1] School of Materials Science and Engineering, Shanghai University, Shanghai 200444, PR China.
[2] Research Center for Functional Materials, National Institute for Materials Science (NIMS), Namiki 1-1, Tsukuba, Ibaraki 305-0044, Japan.
[3] Zhejiang Institute of Advanced Materials, SHU, Jiashan 314113, PR China.
[4] School of Engineering, The University of Leicester, Leicester, LE1 7RH, United Kingdom

Corresponding authors: Zilong Zhang (ZHANG.Zilong@nims.go.jp or zlzhang16@hotmail.com) and Jian Huang (jianhuang@shu.edu.cn)

Abstract

The control of the interface states between the electric contacts and semiconductor is a key issue to develop high-performance functional devices. The polishing, passivation, and oxidation processes can optimize the surface states of the CdZnTe (CZT) film to improve the contact characteristics with the electrode and tailor the resistivity to control the electrical performance. In this work, a serial of surface treatments including mechanical polishing (MP) + chemical polishing (CP) + surface passivation (SP) were conducted to improve the surface states of the CZT film. A transparent Ga-doped Zinc oxide (GZO) was used as the electrode to fabricate the metal-semiconductor-metal (MSM) CZT-based device. The surface treatments of MP, CP, and SP greatly improved the surface contact between CZT films and GZO electrodes. By controlling the thickness of Te oxide layers on CZT film surfaces through

the atmospheric oxidation (AO) and the no-atmospheric oxidation (NAO), the thicknesses of oxide layers on CZT film surfaces were adjusted. The X-ray photoelectron spectroscopy (XPS) was used to observe the oxidation sate of the Te oxide layer. The thickness of the Te oxide layer of CZT film surface in atmosphere environment was evaluated as 18~20 nm through the in-situ XPS measurement, while that of the CZT film in insolated atmosphere was 5~7 nm. In contrast, the CZT film-based device under the combination treatments of MP + CP + SP + AO exhibit a surface roughness of ~4 nm, leading to a significant reduction in the leakage current. The present work provides a strategy to control the thickness of Te oxide layer of the CZT film surface and fabricate a device with a lower current.

Keywords：CdZnTe film; GaZnO film; Surface contact; Oxide layer; XPS technique

1. Introduction

Cadmium zinc telluride (CdZnTe, CZT) has a wide and adjustable band gap (1.45-2.26), high average atomic number, high resistivity and facile fabrication process, which make it as a promising material in the applications of particle radiation detectors, health caring diagnosis and photodetectors [1-3]. Ultraviolet (UV) photodetectors have garnered significant interest due to their widespread applications in industrial, environmental, and biological fields [4-10]. Particularly, the CZT-based detectors have recently attracted increasing attention for UV photodetection due to its high quantum efficiency, high chemical stability, high mobility-lifetime product and simple growth process [2, 3, 11-13]. Furthermore, the performance of a MSM CZT-based photodetector depends not only on its film quality but also on the interface condition between the film and the electrode [14-16]. In fact, the existence of high concentration of interface states between the CZT film and the electrodes and the poor thermal mismatch between the CZT film and the substrate hamper the development of CZT-based device with high performance [3, 12]. In order to circumvent the mismatch of thermal dissipation between the as-deposited CZT film and substrate, a serial of materials including fluorine-doped tin oxide (FTO) glass, indium-doped tin oxide (ITO) glass, GaN, AlN, GaAs and Si were utilized as the substrates to grow CZT films [11, 17-20]. Furthermore, the surface treatments, including mechanical polishing (MP), chemical polishing (CP) and surface passivation (SP) were developed to tailor the surface morphology, roughness, and surface passivation layer. Zhang et al. used

MP+CP+SP treatments to obtain a CZT-based UV detector with a high photocurrent-to-dark current ratio of ~100 [3]. Tari et al. investigated that CP significantly altered the surface morphology, roughness and structure of CZT [14]. Marchini et al. studied that leakage currents can be reduced and contact stability improved by SP [21]. Park et al. reported that SP could affect the metal-semiconductor contact, and in return, enhance the peak-to-valley ratio of the energy spectrum [22]. Sang et al. proposed a novel two-step CP leads to a lower surface leakage current [23]. In order to achieve high electrical performance through reducing the CZT surface roughness to enhance the adhesion with electrodes and increasing the resistance to reduce the leakage current, the combination of MP, CP, and SP treatments were usually adopted [3, 14, 24].

Alternatively, the high-quality contact with little interface states and high barrier height between the CZT film and the electrode is essential for CZT film-based detectors with high performances. Through surface treatments, the interface state of the electrode/CZT interface is greatly reduced. Furthermore, the barrier height of the electrode/CZT is determined by the thickness of surface oxide layer of the CZT film. Recently, a serial of researches pay more attention on the contact characteristics including the enhancement of the geometric contact and the improvement of the contact resistance between metal electrodes and CZT films [3, 11, 13, 25]. In addition, electrode materials are usually opaque Au, Al, Pt, etc. However, the optical reflection in the metal electrodes reduce the light exposure area and photo-response quantum efficiency. Transparent conductive oxide (TCO) thin films are promising candidates for

photodetector to reduce the optical reflection by the electrodes. Ga-doped ZnO (GZO) thin film, a transparent conductive film, hosts the merits of good conductivity, similar thermal expansion coefficient, low cost, as well as facile fabrication process [26, 27]. These merits afford GZO as a promising material to fabricate an electrode for CZT film-based devices [1, 28]. The oxidation behavior at interface between the GZO film and the CZT film plays a critical role in determining the interface states of a CZT film-based device.

In this work, the CZT-based devices with the MSM structure were fabricated on the glass substrates by the close-spaced sublimation (CSS) system and the magnetron sputtering technique to investigate the oxidation of CZT film with and without the atmospheric oxidation (AO). The XPS technique was utilized to investigate the oxidation behavior. The CZT film with the GZO electrodes in lateral view was designed to examine the electrical performance. Furthermore, *I-V* characteristics of CZT film-based devices under various surface treatments were examined. As a result, the CZT film exposed to atmosphere environment produces the oxide layer with a thickness of 18~20 nm, while that of the CZT film in isolated atmosphere environment is 5~7 nm. The CZT-based device under the surface combination treatments involving MP + CP + SP + AO exhibits a low dark current as low as 9.3×10^{-8} A @1 V due to its adaptive thickness of oxide layer and less surface defects. The regulation of the thickness of oxide layer between the CZT and the electrode by surface treatments provides a useful approach to enhance the electrical performance of the CZT-based devices.

2. Experimental

2.1 Films deposition and device fabrication

In this work, CZT films were deposited on 2 × 2 cm^2 ($L \times W$) fluorine-doped tin oxide (FTO) glass substrates by CSS methods. The growth process for the CZT film was discussed in detail in our pervious works [1, 29, 30]. Before the deposition of the CZT films, the FTO glass substrates were sequentially cleaned in acetone, ethanol, and deionized water for 5 min each. Then, they were dried by using a N_2-gun in a clean-room. The CZT films were grown on the FTO glass substrates with a working pressure of 4 Pa, a substrate temperature of 400℃, a target source temperature of 600℃, and a growth duration of 3 h. The composition of the CZT target was $Cd_{0.9}Zn_{0.1}Te$, purchased from Hefei Kejing Materials Technology Co.,Ltd, China. After the deposition of CZT film, the CZT/glass sample was exposed in atmospheric condition for 12 h to produce the natural oxidation. This sample was utilized to examine the oxidation behavior of CZT film with AO treatment. Furthermore, another CZT/glass sample was kept in the vacuum chamber to avoid the atmospheric oxidation. Then, GZO films were grown on CZT/glass substrates through the RF magnetron sputtering system (MSP-300B). The composition of the GZO ceramic target is Ga_2O_3: ZnO=2: 98 (wt%). The basic pressure before the growth process was lower than 10^{-4} Pa. The growth parameters are: a working pressure of 0.9 Pa, a sputtering power of 50 W, a substrate temperature of 300℃ and a growth duration of 70 min. The formation of the GZO/CZT interface was proposed to observe the oxidation of the CZT film without the atmosphere oxidation.

Alternatively, the mechanical polishing (MP) was carried out on the as-deposited CZT films by using 50 nm-size Al_2O_3 particles for 3 h. The polishing particles were uniformly dispersed in a polishing cloth with fluff. The same process of MP treatment for the CZT film was utilized in our previous work [3, 30]. Then, the as-MP treated CZT film was subjected to the chemical polishing (CP) under 2 vol% Br-MeOH solution with the etching duration of 1 min. Furthermore, a surface passivation (SP) layer was produced by the passivating treatment in NH_4F (10 wt%) + H_2O_2 (10 wt%) for 10 min. The GZO electrodes were produced on the as-surface treated CZT films with and without the AO treatment *via* the magnetron sputtering technique. The various kinds of samples treated by different surface treatments are shown in Table 1. The GZO/CZT/GZO structure in the lateral view was utilized to examine the electrical performance. The GZO electrode structure is characterized as an interdigitated finger width of 0.5 mm, length of 10 mm and an interval of 1 mm. The thicknesses of the GZO electrode and the CZT film are 180 nm and 220 nm.

Table 1 Various samples treated by different surface treatments

Samples	**Surface treatments**
T1	Mechanical polishing (MP)+ Atmospheric oxidation (AO)
T2	MP+ Chemical polishing (CP)+AO
T3	MP+ Surface passivation (SP)+AO
T4	MP+CP+SP+AO
T5	MP+ non-atmospheric oxidation (NAO)

T6	MP + CP + NAO

2.2 Characterization

The surface morphologies of the CZT films with various surface treatments were examined by atomic force microscope (AFM) and scanning electron microscope (SEM, JSM-7500F). The phase structures of the CZT films were analyzed *via* X-ray diffraction (XRD) system by using Cu Ka radiation (λ = 1.54 Å). The composition and film quality of CZT films were measured by Raman spectrometer (Horiba Jobin Yvons, HR800UV) system, which is excited by 514.5 nm Ar^+ wavelength laser with a spot diameter of 2 μm and a power of 1 W. X-ray photoelectron spectroscopy (XPS) analysis was performed by using Thermo ESCALAB 250Xi X-ray photoelectron spectroscopy equipped with Al *Kα* radiation (*hv* = 1486.6 eV) at a power of 150 W and a beam spot diameter of 500 μm. The electrical properties of these detectors were measured by using a Keithley 4200A-SCS (Semiconductor Characterization System) Parameter Analyzer.

3. Results and discussion

3.1 Microstructures of CZT films under various surface treatments

The AFM profiles of surface morphologies and roughness of CZT films under different surface treatments are shown in Fig. 1(a-d). The CZT films are named as T1~T4, as shown in **Table 1**. Some scratches appear on T1 surface as shown in Fig. 1(a) due to the MP treatment. It can be seen that the preferential etching is occurred for T2 sample with a relative high roughness value compared to that of T1 sample, as depicted

171 in Fig. 1(b). The appearance of the increasing in surface roughness is effectively
172 eliminated by a layer produced from the SP treatment. For the T3 sample, although it is
173 subjected to the SP treatment, the surface morphology is similar to that of T1 sample,
174 as shown in Fig. 1(c). The surface scratches of T4 sample are basically removed,
175 resulting in the good surface condition with a small roughness value, as shown in Fig.
176 1(d). Fig. 1(e) shows the XRD patterns of the CZT films with different surface
177 treatments, demonstrating the main (111)-orientation of these CZT films. T4 sample
178 exhibits good surface quality due to the higher diffraction intensity. The crystal
179 structure parameters of various samples are listed in **Table S1** (Supplementary material).
180 The 2θ of (111)-orientation shift with the various surface treatment. It is disclosed that
181 this shift shows weak dependence on the surface treatments. It can be seen that the full
182 width at half maximum (FWHM) of the CZT film under CP treatment is larger than that
183 of CZT film under merely MP treatment. The SP treatment is beneficial for reducing
184 FWHM after the CP treatment. The Raman spectra of CZT films are show in Fig. 1(f).
185 The peak at 123 cm^{-1} corresponds to Te element-related A_1 mode, and the peak at 140
186 cm^{-1} corresponds to CZT-related TO_1 (The transverse phonon oscillates) and Te
187 element-related E_1 mode [29, 31-33]. The peaks at around 100 cm^{-1} and after 200 cm^{-1}
188 represent the E_{TO} (Te) mode and the LO_2 (ZnTe) mode, respectively. No peaks of CdTe
189 and ZnTe and other impurities are observed, indicating the good quality for as-grown
190 CZT film. As we know, the peak intensity of Raman spectrum can be utilized to indicate
191 the content of vibrating groups of materials [34, 35]. It can be seen that the peak

intensities of T3 and T4 samples are significantly higher than that of T1 and T2 samples, which demonstrates that these dense oxide films with high activity and content of vibrating groups are formed on CZT film surfaces through the SP treatment. Furthermore, T1 and T2 samples appear the peak at 166 cm^{-1} with weak intensity, corresponding to the CZT-related LO_1 (the longitudinal phonon oscillates) [31, 33].

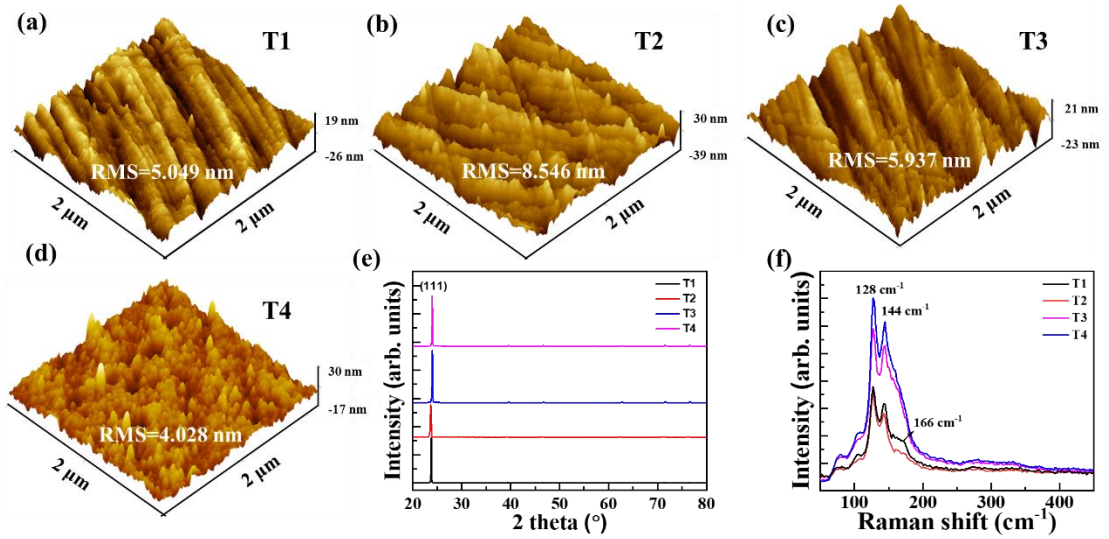

Fig. 1. (a-d) AFM images of CZT films after different surface treatments. T1 sample: under mechanical polishing (MP) + atmospheric oxidation (AO). T2 sample: under MP + chemical polishing (CP) + AO. T3 sample: MP + surface passivation (SP) + AO. T4 sample: under MP + CP + SP + AO. (e-f) XRD and Raman spectra of the CZT films after different surface treatments.

3.2 Observation of oxidation behavior of CZT films through XPS tests

In this work, the XPS technique was applied for examining the existence and thickness of surface oxide layer of the CZT film exposed to the atmosphere condition. The fabrication of the GZO/CZT interface was also proposed to observe the oxidation

208 of the CZT film without the atmosphere oxidation. Before the XPS measurement, the
209 CZT film was subjected to the MP treatment. The SEM image of the cross-section of
210 GZO/CZT structure is shown in Fig. 2(a). It can be seen that the GZO film exhibits a
211 uniform and dense columnar morphology. An abrupt interface was observed in the
212 GZO/CZT contact interface. Fig. 2(b) depicts the schematic diagram of Ar ion etching
213 treatment of the GZO/CZT structure for the XPS measurement. The Ar ion is utilized
214 to etch the GZO film and the CZT film. The etching process was carried out on the
215 sample surface with an etching rate of 0.7 nm/s, which was checked by the standard
216 sample of tantalum pentoxide. The etching process and obtaining spectrum were
217 performed alternately. The binding energies of the elements involved in the XPS
218 measurement are listed in **Table S2**, which was utilized to judge the chemical states of
219 the elements [36]. To some extent, the contents and valence states of different elements
220 from different depths can be utilized to distinguish the materials in the certain area of
221 the GZO/CZT structure.

222 Figure 2(c) shows the photoelectron spectra of Te elements at three etching
223 positions of as-MP CZT film, which is exposed in the atmosphere. Due to the different
224 chemical environments of Te atoms, two peaks of Te $3d_{5/2}$ and Te$3d_{3/2}$ with binding
225 energies of 572.6 eV and 583.1 eV, respectively, are appeared for Te element in the form
226 of CZT. It can be seen that this peak intensity at 572.6 eV and 583.1 eV increases with
227 the etching depth increasing from 120 s to 180 s, which confirms that the content of Te
228 element in the form of CZT is increased. Alternatively, two peaks of Te $3d_{5/2}$ and Te

229 $3d_{3/2}$ (oxidation state) with binding energies of 576.2 eV and 586.6 eV, respectively,
230 emerge in the XPS spectrum as the etching time of 120 s. According to **Table S2**, these
231 two above peaks with higher binding energies are from the Te oxide. Moreover, these
232 two oxide peaks basically disappear when the etching time reached 135 s and 180 s.
233 Therefore, a native Te oxide was confirmed to be formed in atmosphere condition.
234 Based on the etching rate, the thickness of the atmospheric oxide layer of the CZT film
235 is evaluated to be 18~20 nm with the etching durations of 120~130 s.

236 Furthermore, in order to explore the existence of the oxide layer on this CZT film
237 surface, the photoelectron spectra of O elements with the etching time of 120 s and 180
238 s were analyzed, respectively, as shown in Fig. 2(d). When the etching time is 120 s,
239 the O 1s spectrum shows two separated peaks, namely, O1s scanA and O1s scanB [37,
240 38]. It is indicated that there are two different electron states in the 1s orbital of O
241 element. The binding energies of O1s scanA and O1s scanB are fitted to be 529.8 eV
242 and 531.3 eV, respectively. From **Table S2**, scanA and scanB represent the 1s electron
243 peak of O element in the Te oxide and the electron peak from the OH^-/H_2O, respectively.
244 The fitted higher binding energy of the O1s spectrum is close to that of scanA, which
245 is mainly from the Te oxide. The binding energy of O1s peak at the longer etching time
246 of 180 s is 530.3 eV, indicating the binding energy of adsorbent containing oxygen,
247 which may be formed in the chamber. The peak intensity decreased with increasing the
248 binding energy, indicating the content of Te oxide is higher than that of the adsorbent
249 containing oxygen. It illustrates that the content of Te oxide in the CZT film decreases

with the etching depth increasing, which is consistent with the photoelectron spectrum of Te element in Fig. 2(c).

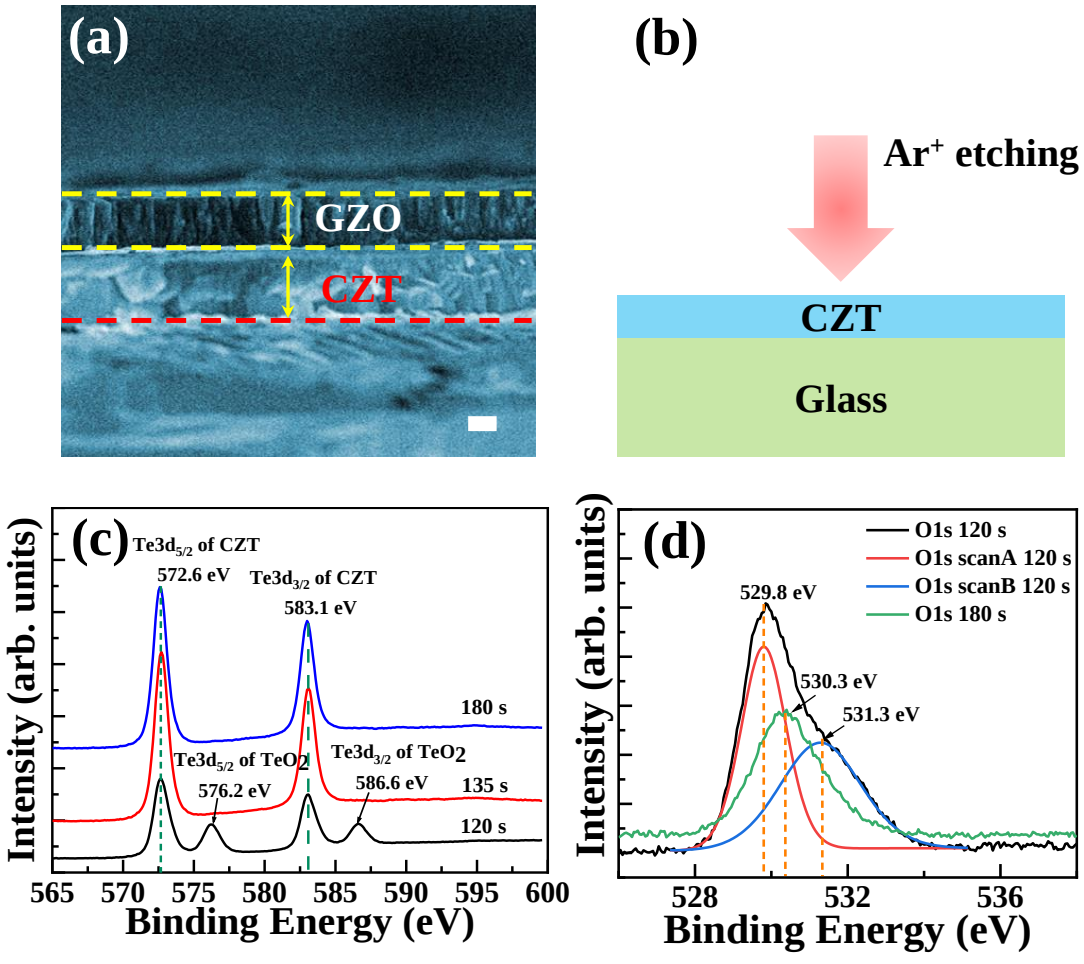

Fig. 2. (a) SEM image of cross-section of the GZO film grown on the CZT film. Scale bar: 80 nm. (b) Schematic diagram of in-stiu XPS test of as-MP CZT surface under the Ar ion etching. Depth imaging XPS spectra of (c) Te photoelectron and (d) O photoelectron of as-MP CZT film under various etching durations.

Based on the existence of the Te oxide on the CZT film surface with AO treatment through the photoelectron spectra of Te and O elements, the depth distributions of full elements with the etching duration were analyzed by the XPS system, as shown in Fig.

3(a). Furthermore, in order to examine the existence of oxide layer and its thickness of the GZO/CZT contact interface, the composition and characteristics of each element at the GZO/CZT interface were analyzed via the Ar ion etching. The etching rate for GZO film can be calculated based on the etching rate of standard sample, which is utilized to estimate the thickness of contact interface. Fig. 3(a) exhibits the schematic diagram of XPS test of the GZO/CZT interface through Ar ion etching. The depth distributions of full elements of the GZO/CZT interface were also analyzed by the XPS system, as shown in Fig. 3(b). It can be observed that there are co-existences of Zn, Ga and O elements as the etching duration lower than 360 s. During the etching duration of 360 s to 400 s, the Cd element begins to appear and its relative proportion increases with the etching duration. The relative proportion of Ga element maintains weak change. The relative proportions of Zn and O elements decrease with the etching duration. Furthermore, the relative proportion of Te element (oxidation state) first increases and then decreases to zero with the etching duration increasing. During the etching durations from 390 s to 400 s, the Te element (bulk state) begins to appear and its relative proportion increases with the etching duration. The relative proportion variations of elements amongst the etching duration from 360 s to 400 s indicates that the etching thickness in this etching interval is the thickness of oxide layer, which is estimated to be about 5~7 nm based on the etching rate. According to the variations of elements, Fig. 3(c) schematically shows the distribution of substances on the GZO/CZT interface.

In order to further analyze the reason of the existence of Te oxide at the GZO/CZT interface, the XPS spectra of Te element at this interface are depicted in Fig. 3(d). It shows that at the etching duration of 360 s, the electron peaks of Te elements (oxidation state and bulk state) exhibit weak intensities, which illustrates this examined area is in GZO film. With the etching duration increasing, the electron peaks of Te elements with the oxidation state of 571.4 eV and the bulk state of 581.7 eV appear during the etching durations of 375~400 s. As the etching duration larger than 400 s, the electron peak of Te element (oxidation state) basically disappears, while the peak intensity of Te element (bulk state) is significantly enhanced, which demonstrates this examined area is in the CZT film. In overall, in view of the XPS spectra of Te elements, it can be obtained that the existence of weak permeation diffusion and chemical reaction in GZO/CZT interface, which is consistent with the result in Fig. 3(b).

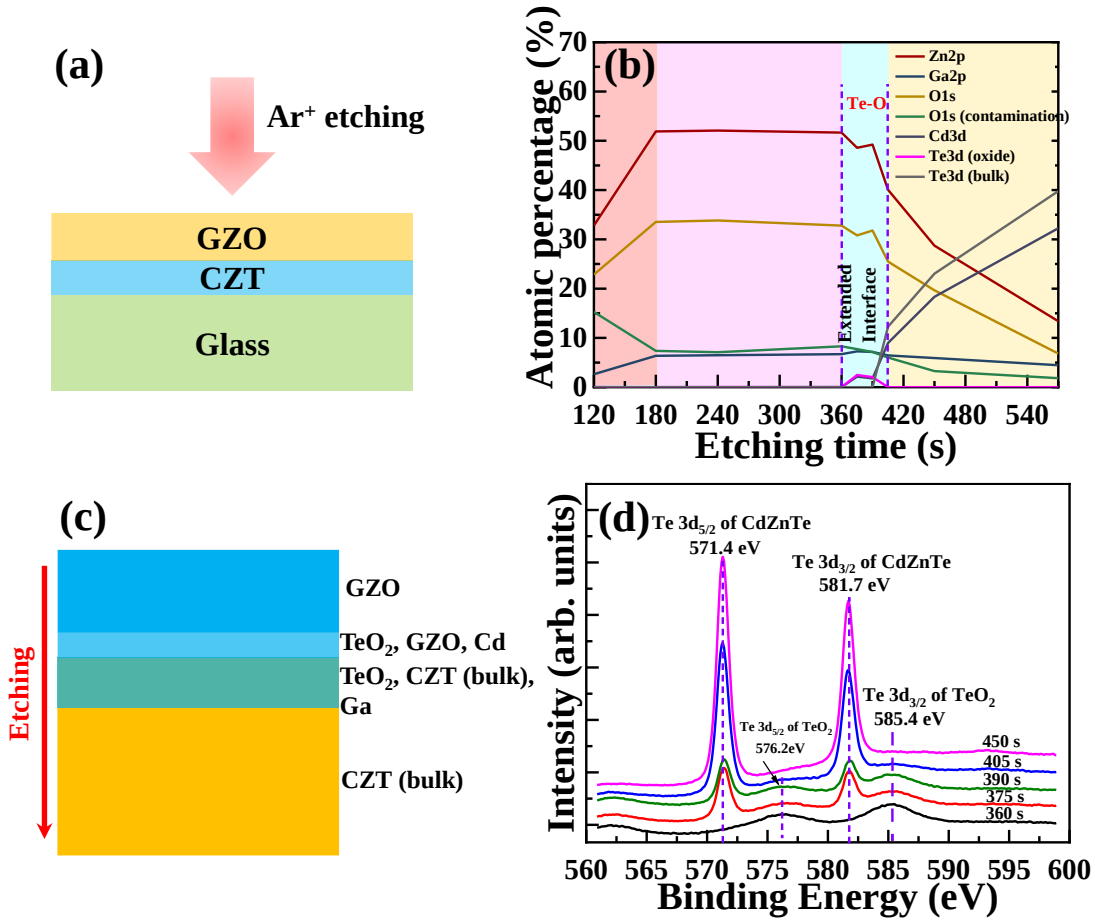

Fig. 3. (a) Schematic diagram of XPS test of the GZO/CZT structure under the Ar ion etching. (b) Dependences of atomic percentage of full elements in the GZO/CZT interface on different etching durations. (c) Schematic diagram of element distribution inthe GZO/CZT structure. (d) Depth profiling XPS spectra of Te element in the GZO/CZT structure with different etching durations.

3.3 Electrical performance of GZO/CZT/GZO structure device

As discussed in 3.2 chapter, it can be obtained that the CZT film exposed to the atmosphere environment produced the oxide layer with a thickness of 18~20 nm, while that of the CZT film in the GZO/CZT structure is significantly limited due to the weak

interaction at interface, showing the thickness is 5~7 nm. In the CZT-based device, the thicknesses of the GZO electrode and the CZT film are 180 nm and 220 nm. In general, the electrical performance of a GZO/CZT/GZO device is determined by the GZO/CZT interface states. The interface states and barrier height between the CZT film and the electrode show strong relationship with the thickness of oxide layer of CZT film. The GZO film exhibits a bright promising to act as an electrode material for a CZT film-based device due to the controlled thickness of oxide film in the GZO/CZT structure. The aim of these electrical measurements is to figure out the suitable surface treatments to fabricate the UV CZT-based photodetector with a low dark current, which is in favor of achieving high photodetection performance. In our previous work, the surface state of the CZT film can be tailored through the surface treatments [3]. Here in this study, the influence of the oxide layer on electrical performance of CZT film-devices after various surface treatments was examined. Furthermore, after these surface treatments, two CZT films were kept in the vacuum chamber to avoid the atmosphere, as called T5 sample (subjected to MP+ non-atmospheric oxidation (NAO)) and T6 sample (subjected to MP + CP + NAO). Fig. 4(a) exhibits the schematic diagram of a CZT-based devices with the interdigital GZO electrodes. The photo image of a CZT-based detector is shown in Fig. S1. In addition, Fig. 4(b) depicts the *I-V* plots of CZT film-devices with different surface treatments, demonstrating that the dark-currents vary with the applied voltage. The dark current is utilized to reflect the contact performance for these devices after various surface treatments. The low dark current indicates the

good contact in the interface with low defects. For T1 sample, the device has a low dark current. The *I-V* curve of T2 sample has good symmetry feature. The dark current is obviously larger than that of T1 sample due to the enrichment of Te element on the CZT surface after CP treatment [3]. T3 sample also has a large dark current. The T4 sample possesses low dark current od ~9.3×10^{-8} A @1 V. Compared with the dark currents of T3 sample and T4 sample, it can be obtained that the SP on the CZT film surface after MP + CP treatments is more beneficial to reduce the surface states. This is due to that the CP treatment can smooth the CZT film surface, remove surface damage, and form the stable oxide layer. Furthermore, the *I-V* plot of T5 sample exhibits a high dark current. It indicates the existence of weak interaction between the GZO electrode and as-MP CZT film with the NAO treatment. The more capture energy levels caused by interface defects lead to the dark current increasing. The dark current of T6 sample sharply increases due to an obvious decrease in surface resistance. After MP + CP + NAO treatments, the CZT film exhibits a very poor interface state, which results in the serious deterioration of stoichiometry. Thus, the CZT film suffered from the NAO treatment is not suitable for fabricating the CZT-device with a low dark current.

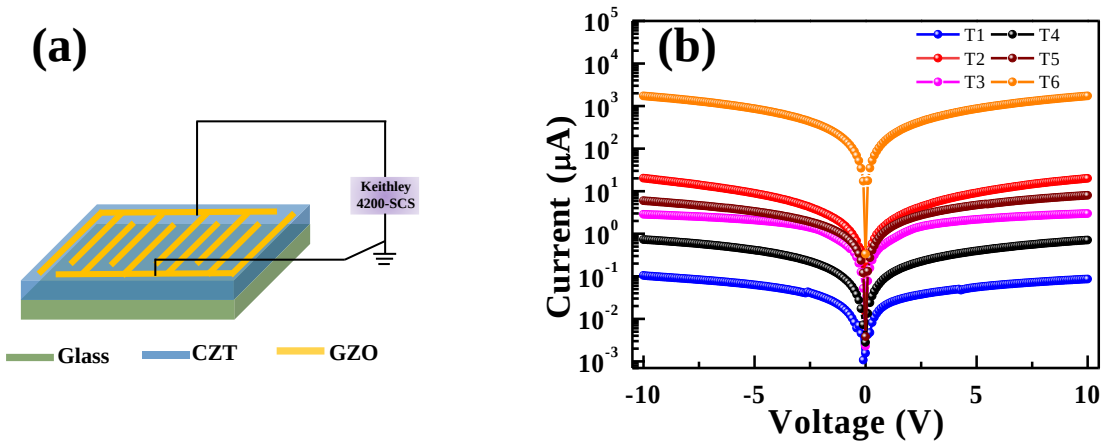

Fig. 4. (a) Schematic setup of a CZT-based UV device. (b) Dependences of dark current on the applying voltage at dark conditions.

Based on the *I-V* plots of the CZT film-based detectors under various surface treatments, it can be seen that the existence of the Te oxide layer and its thickness play a critical influence on the electrical performance. The Te oxide layer is in favor of limiting the dark current. For the T1 sample with MP + AO treatments, it can produce the adequate oxide layer on film surface, which results in the highest barrier height and the lowest dark current. The thickness of the oxide layer under the AO treatment is evaluated as a value of 18~20 nm. The SP treatment can circumvent the issue of the Te enrichment on the film surface due to the CP treatment (see $I_{T3} < I_{T2}$). The T4 sample with the combination of surface treatments involving MP + CP + SP + AO treatments exhibits the low dark current due to its adaptive thickness of oxide layer and good surface state. These T5 and T6 samples with the NAO treatment have limited thickness of oxide layer and the low barrier height, which leads to the large dark current. The AO treatment is beneficial for the CZT film to obtain the suitable thickness of oxide layer

and optimal barrier height.

4. Conclusion

In summary, CZT films were grown on FTO glass substrates by the CSS system. The oxidation behaviors of these CZT films with and without the AO treatment were observed through the XPS technique. The results show that the thickness of oxide layer of the CZT film surface exposed to atmosphere environment is evaluated as 18~20 nm, while that of the CZT film in the GZO/CZT structure with NAO treatment was 5~7 nm. The surface treatments, including MP, CP and SP are utilized to reduce the surface roughness and improve the surface condition to obtain a better adhesion and contact between the GZO and the CZT. Furthermore, the large thickness of oxide insulating layer is in favor of increasing the resistance and reducing dark current. The CZT-based device with surface combination treatments of MP + CP + SP + AO exhibits a low dark current of 9.3×10^{-8} A @1 V, which is essential for the fabrication of devices with high signal-to-noise ratio. The regulation of oxide layer on the CZT film surface offers a promising strategy for fabricating CZT-based devices with high electrical performance.

Declaration of Competing Interest

The authors declare that they have no known competing financial interests or personal relationships that could have appeared to influence the work reported in this paper.

Acknowledge

This work was funded by National Science Foundation of China (No. 11875186 and No. 11905121, No. 11775139).

References

[1] T. Zou, J. Huang, Y. Hu, K. Tang, Z. Zhang, X. Zhou, Y. Shen, J. Zhang, L. Wang, Y. Lu, CdZnTe thick film radiation detectors with B and Ga co-doped ZnO contacts, Surf. Coat. Technol., 360 (2019), 64-67.

[2] S.N. Moger, M. Mahesha, Investigation on ZnTe/CdxZn1-xTe heterostructure for photodetector applications, Sens. Actuator A Phys., 315 (2020), 112294.

[3] Z. Zhang, K. Gu, F. Yang, J. Huang, K. Tang, Y. Shen, J. Zhang, M. Liao, L. Wang, Enhanced UV detection performance of a CdZnTe-based photodetector through surface polishing treatments, J. Mater. Chem. C, 9(10) (2021), 3601-3607.

[4] H. Yang, S. Cai, Y. Zhang, D. Wu, X. Fang, Enhanced electrical properties of lithography-free fabricated MoS2 field effect transistors with chromium contacts, The J. Phys. Chem. Lett., 12(11) (2021), 2705-2711.

[5] Z. Li, T. Yan, X. Fang, Low-dimensional wide-bandgap semiconductors for UV photodetectors, Nat. Rev. Mater., (2023), 1-17.

[6] X. Xu, J. Chen, S. Cai, Z. Long, Y. Zhang, L. Su, S. He, C. Tang, P. Liu, H. Peng, X. Fang, A real-time wearable UV-radiation monitor based on a high-performance p-CuZnS/n-TiO_2 photodetector, Adv. Mater. 30(43) (2018), 1803165.

[7] Y. Chen, L. Su, M. Jiang, X. Fang, Switch type PANI/ZnO core-shell microwire heterojunction for UV photodetection, J. Mater. Sci. Technol., 105 (2022) 259-265.

[8] M. Deng, Z. Li, X. Deng, Y. Hu, X. Fang, Wafer-scale heterogeneous integration of self-powered lead-free metal halide UV photodetectors with ultrahigh stability and homogeneity, J. Mater. Sci. Technol., 164 (2023), 150-159.

[9] M. Liao, Progress in semiconductor diamond photodetectors and MEMS sensors, Functional Diamond 1(1) (2022), 29-46.

[10] M. Imura, M. Togawa, M. Miyahara, H. Okumura, J. Nishinaga, M. Liao, Y. Koide, Highly tolerant diamond Schottky barrier photodiodes for deep-ultraviolet xenon excimer lamp and protons detection, Functional Diamond 2(1) (2022), 167-174.

[11] Y. Shen, Y. Xu, J. Sun, Z. Zhang, J. Huang, M. Cao, F. Gu, L. Wang, Interface regulation and photoelectric performance of CdZnTe/AlN composite structure for UV photodetector, Surf. Coat. Technol. 358 (2019), 900-906.

[12] J. Sun, Y. Shen, R. Chen, J. Huang, M. Cao, F. Gu, L. Wang, J. Min, Effect of ZnTe

transition layer to the performance of CdZnTe/GaN multilayer films for solar-blind photodetector applications, J. Phys. D: Appl. Phys. 53(41) (2020), 415105.
[13] M. Shkir, M.T. Khan, I. Ashraf, A. Almohammedi, E. Dieguez, S. AlFaify, High-performance visible light photodetectors based on inorganic CZT and InCZT single crystals, Sci. Rep., 9(1) (2019), 1-9.
[14] S. Tari, F. Aqariden, Y. Chang, C. Grein, J. Li, N. Kioussis, Impact of surface treatment on the structural and electronic properties of polished CdZnTe surfaces for radiation detectors, J. Electron. Mater., 42(11) (2013), 3252-3258.
[15] S. Del Sordo, L. Abbene, E. Caroli, A.M. Mancini, A. Zappettini, P. Ubertini, Progress in the development of CdTe and CdZnTe semiconductor radiation detectors for astrophysical and medical applications, Sensors, 9(5) (2009), 3491-3526.
[16] A. Brovko, A. Adelberg, L. Chernyak, S. Gorfman, A. Ruzin, Impact of polishing on crystallinity and static performance of Cd1-xZnxTe, Nucl. Instrum. Meth. A, 984 (2020), 164568.
[17] S. Chander, M. Dhaka, Optimization of structural, optical and electrical properties of CdZnTe thin films with the application of thermal treatment, Mater. Lett., 182 (2016), 98-101.
[18] S. Chander, M. Dhaka, Enhanced structural, electrical and optical properties of evaporated CdZnTe thin films deposited on different substrates, Mater. Lett., 186 (2017), 45-48.
[19] S. Chander, A. Purohit, S. Patel, M. Dhaka, Effect of substrates on structural, optical, electrical and morphological properties of evaporated polycrystalline CdZnTe thin films, Physica E Low Dimens. Syst. Nanostruct., 89 (2017), 29-32.
[20] J. Gao, W. Jie, Y. Yuan, T. Wang, Y. Xie, Y. Wang, Y. Huang, J. Tong, H. Yu, G. Pan, One-step fast deposition of thick epitaxial CdZnTe film on (001) GaAs by close-spaced sublimation, CrystEngComm, 14(5) (2012), 1790-1794.
[21] L. Marchini, A. Zappettini, E. Gombia, R. Mosca, M. Lanata, M. Pavesi, Study of surface treatment effects on the metal-CdZnTe interface, IEEE Trans. Nucl. Sci., 56(4) (2009), 1823-1826.
[22] S. Park, J. Ha, Y. Cho, H. Kim, S. Kang, Y. Kim, J. Kim, Surface passivation effect on CZT-metal contact, IEEE Trans. Nucl. Sci., 55(3) (2008), 1547-1550.
[23] S. Wenbin, W. Kunshu, M. Jiahua, T. Jianyong, Z. Qi, Q. Yongbiao, A novel two-step chemical passivation process for CdZnTe detectors, Semicond. Sci. Technol., 20(5) (2005), 343.
[24] M. Duff, D. Hunter, A. Burger, M. Groza, V. Buliga, D.R. Black, Effect of surface preparation technique on the radiation detector performance of CdZnTe, Appl. Surf. Sci., 254(9) (2008), 2889-2892.
[25] R. Chen, Y. Shen, T. Li, J. Huang, F. Gu, X. Liang, M. Cao, L. Wang, J. Min, Interface optimization of free-standing CdZnTe films for solar-blind ultraviolet detection: Substrate dependence, Vacuum, 193 (2021), 110484.
[26] T. Nam, C.W. Lee, H.J. Kim, H. Kim, Growth characteristics and properties of Ga-doped ZnO (GZO) thin films grown by thermal and plasma-enhanced atomic layer

458 deposition, Appl. Surf. Sci., 295 (2014), 260-265.
459 [27] S.H. Chang, H.-M. Cheng, C.-L. Tien, S.-C. Lin, K.-P. Chuang, Optical, electrical
460 and mechanical properties of Ga-doped ZnO thin films under different sputtering
461 powers, Opt. Mater., 38 (2014), 87-91.
462 [28] Y. Shen, J. Huang, Q. Gu, H. Meng, K. Tang, Y. Shen, J. Zhang, L. Wang, Y. Lu,
463 The investigation of Ga-doped ZnO as an interlayer for ohmic contact to Cd1-xZnxTe
464 films, Appl. Surf. Sci., 425 (2017), 176-179.
465 [29] J. Huang, Q. Gu, F. Yang, K. Tang, S. Gou, Z. Zhang, Y. Shen, J. Zhang, L. Wang,
466 Y. Lu, Growth and properties of CdZnTe films on different substrates, Surf. Coat.
467 Technol., 364 (2019), 444-448.
468 [30] F. Yang, J. Huang, T. Zou, K. Tang, Z. Zhang, Y. Ma, S. Gou, Y. Shen, L. Wang, Y.
469 Lu, The influence of surface processing on properties of CdZnTe films prepared by
470 close-spaced sublimation, Surf. Coat. Technol., 357 (2019), 575-579.
471 [31] G.A. Kulkarni, V. Sathe, K. Rao, D. Muthu, R. Sharma, Micro-Raman imaging of
472 Te precipitates in CdZnTe (Zn~ 4%) crystals, J. Appl. Phys., 105(6) (2009), 063512.
473 [32] H. Xu, R. Xu, J. Huang, J. Zhang, K. Tang, L. Wang, The dependence of Zn content
474 on thermal treatments for Cd1-xZnxTe thin films deposited by close-spaced
475 sublimation, Appl. Surf. Sci., 305 (2014), 477-480.
476 [33] J. Min, X. Liang, J. Chen, D. Wang, H. Li, J. Zhang, Investigation of Te inclusions
477 in CdZnTe crystalline material using Raman spectroscopy and IR techniques, Vacuum,
478 86(7) (2012), 1003-1006.
479 [34] A.K. Yadav, P. Singh, A review of the structures of oxide glasses by Raman
480 spectroscopy, RSC Adv., 5(83) (2015), 67583-67609.
481 [35] P. Colomban, A. Slodczyk, Raman intensity: An important tool to study the
482 structure and phase transitions of amorphous/crystalline materials, Opt. Mater., 31(12)
483 (2009), 1759-1763.
484 [36] J.F. Moulder, Handbook of X-ray photoelectron spectroscopy, Physical electronics
485 (1995) 230-232.
486 [37] C. Zhang, J. Sunarso, S. Liu, Designing CO_2-resistant oxygen-selective mixed
487 ionic–electronic conducting membranes: guidelines, recent advances, and forward
488 directions, Chem. Soc. Rev., 46(10) (2017), 2941-3005.
489 [38] L. Wu, Y. Li, S. Li, Z. Li, G. Tang, W. Qi, L. Xue, X. Ge, L. Ding, Method for
490 estimating ionicities of oxides using O1s photoelectron spectra, AIP Adv., 5(9) (2015),
491 097210.

492